

**Materials Sciences Division, Lawrence Berkeley National Laboratory, and  
Department of Materials Science and Engineering  
University of California at Berkeley**

**STRESS-CORROSION FATIGUE-CRACK GROWTH  
IN A Zr-BASED BULK AMORPHOUS METAL**

***V. Schroeder\* and R. O. Ritchie***

Materials Sciences Division, Lawrence Berkeley National Laboratory, and  
Department of Materials Science and Engineering,  
University of California, Berkeley, CA 94720, USA

\*currently at Nitinol Devices and Components, Johnson and Johnson,  
Fremont, CA 94539, USA

September 2005

submitted to *Acta Materialia*

Work supported by the Director, Office of Science, Office of Basic Energy Sciences,  
Division of Materials Sciences and Engineering of the U.S. Department of Energy under  
Contract No. DE-AC02-05CH11231.

# STRESS-CORROSION FATIGUE-CRACK GROWTH IN A Zr-BASED BULK AMORPHOUS METAL

*V. Schroeder\* and R. O. Ritchie*

Materials Sciences Division, Lawrence Berkeley National Laboratory, and  
Department of Materials Science and Engineering,  
University of California, Berkeley, CA 94720, USA

**Abstract:** Electrochemical and mechanical experiments were conducted to analyze the environmentally-influenced cracking behavior of a bulk amorphous metal,  $Zr_{41.2}Ti_{13.8}Cu_{12.5}Ni_{10}Be_{22.5}$ . This study was motivated by a scientific interest in mechanisms of fatigue-crack propagation in an amorphous metal, and by a practical interest in the use of this amorphous metal in applications that take advantage of its unique properties, including high specific strength, large elastic strains and low damping. The objective of the work was to determine the rate and mechanisms of subcritical crack growth in this metallic glass in an aggressive environment. Specifically, fatigue-crack propagation behavior was investigated at a range of stress intensities in air and aqueous salt solutions by examining the effects of loading cycle, stress-intensity range, solution concentration, anion identity, solution de-aeration, and bulk electrochemical potential. Results indicate that crack growth in aqueous solution in this alloy is driven by a stress-assisted anodic reaction at the crack tip. Rate-determining steps for such behavior are reasoned to be electrochemical, stress-dependent reaction at near-threshold levels, and mass transport at higher (steady-state) growth rates.

*Key words:* Bulk metallic glass, amorphous metal, fatigue, stress-corrosion, crack growth

## **I. Introduction**

In recent years, several families of multi-component metallic alloys have been developed that exhibit exceptional glass-forming ability. These alloys show a very high resistance to crystallization in the undercooled liquid state, such that relatively slow cooling rates (typically less than 10 K/s) can be employed to achieve fully amorphous structures. Since these amorphous structures can now be processed in large sections, bulk metallic glasses have been formed. These glasses have gained interest based on claims of near-theoretical

---

\* currently at Nitinol Devices and Components, Johnson and Johnson, Fremont, CA 94539.

strength-to-stiffness ratios, large elastic deflections, low damping characteristics, good wear properties, and a potential for easy forming and shaping. One notable monolithic alloy of study has been Vitreloy 1<sup>1</sup>, with a composition (in at.%) of  $Zr_{41.2}Ti_{13.8}Cu_{12.5}Ni_{10}Be_{22.5}$ , which has been developed commercially and is used, in its fully amorphous state, in the manufacture of golf clubs. Although the mechanical performance of this alloy has been well documented and is known to show satisfactory fracture toughness and fatigue-crack growth resistance [1-5], its corresponding properties in the presence of a corrosive environment have been far less impressive [6]. Indeed, amorphous  $Zr_{41.2}Ti_{13.8}Cu_{12.5}Ni_{10}Be_{22.5}$  has been shown to be highly susceptible to stress-corrosion cracking and stress-corrosion fatigue in the presence of aqueous sodium chloride solution [6].

It is the purpose of the current study to examine in detail the stress-corrosion fatigue of the amorphous  $Zr_{41.2}Ti_{13.8}Cu_{12.5}Ni_{10}Be_{22.5}$  alloy in aqueous environments, by considering the separate roles of loading cycle, stress-intensity range, solution concentration, anion identity, solution de-aeration, and bulk electrochemical potential on the crack-growth behavior.

## II. Background

A number of amorphous metals exhibit excellent corrosion resistance [7-10], which has been ascribed to their structural and chemical homogeneity. Indeed, the corrosion resistance in amorphous metals has been attributed to the presence of a highly stable passive film, concentrated in certain alloying elements known to provide good corrosion resistance in crystalline metals.

Most studies on stress-corrosion cracking (SCC) of amorphous metals in aqueous solutions have focused on thin ribbon material, where constant displacement experiments have been used to evaluate environmentally-assisted fracture. For example, iron-based amorphous metals with good resistance to pitting corrosion in the absence of load were found to exhibit stress-corrosion cracking in acidic chloride-containing environments [11-15]. Specifically, these alloys, particularly when they contained high concentrations of chromium, exhibited stress-corrosion behavior comparable to that of unsensitized stainless

---

<sup>1</sup> Vitreloy 1 is a trademark of Amorphous Technologies International, Corp.

steels [11]. Fracture surfaces resulting from these tests displayed a brittle appearance [11] and, in some cases significant crack branching [12]. While these experiments provide some information about stress-corrosion cracking in amorphous metals, crack initiation was not controlled and crack velocities and stress intensities at the crack tip during crack growth were not measured. As a result, the effect of solution on crack initiation could not be separated from its effect on crack propagation.

For the bulk amorphous alloy  $Zr_{41.2}Ti_{13.8}Cu_{12.5}Ni_{10}Be_{22.5}$ , controlled stress corrosion and stress-corrosion fatigue-crack growth behavior have both been measured in 0.5 M NaCl solution [6]. Based on this study, it has been found that aqueous sodium chloride solution causes very significant stress-corrosion cracking and stress-corrosion fatigue effects in this alloy, most especially by dramatically increasing crack-growth rates by approximately two orders of magnitude compared to corresponding growth rates in air or de-ionized water. It is the objective of the current paper to provide further information on the nature of this environmentally-assisted cracking phenomenon in the Zr-based bulk amorphous alloy.

### III. Experimental Procedures

Experiments were performed on as-cast 7-mm thick plates of the fully amorphous alloy  $Zr_{41.2}Ti_{13.8}Cu_{12.5}Ni_{10}Be_{22.5}$  in at.% ( $Zr_{62.6}Ti_{10}Cu_{13.2}Ni_{9.8}Be_{3.4}$  in wt.%). The castings were processed by Hitchener Manufacturing Co. (Milford, NH) and provided by Amorphous Technologies International, Corp. (Laguna Niguel, CA). Typical mechanical and physical properties are given in Table 1.

**Table 1:** Mechanical and physical properties of  $Zr_{41.2}Ti_{13.8}Cu_{12.5}Ni_{10}Be_{22.5}$  bulk metallic glass

Density (g/cm <sup>3</sup> )	Young's Modulus (GPa)	Shear Modulus (GPa)	Poisson's Ratio	Yield Strength (GPa)	Vickers Hardness (GPa)	Fracture Toughness (MPa√m)	Glass Transition (K)
5.9	95	35	0.35	1.9	5.4	~20	~625

Compact-tension (C(T)) specimens of the amorphous alloy were fabricated by electro-discharge machining to a thickness of 4.4 mm and a width of 20 mm. To insure

that the compressive residual stresses present in the surface layers of the casting [1] did not affect behavior, at least 1.5 mm of material was removed from all surfaces.

Fatigue testing was conducted at room temperature ( $\sim 22^{\circ}\text{C}$ ) in several environments:

- laboratory air (relative humidity  $\sim 25\text{-}35\%$ ),
- aerated de-ionized water,
- aerated 0.5 M  $\text{NaClO}_4$  (99+%, EM Science) solution in de-ionized water,
- aerated 0.5 M  $\text{Na}_2\text{SO}_4$  (99+%, J. T. Baker) solution in de-ionized water,
- aerated 0.005 M NaCl, 0.05 M NaCl and 0.5 M NaCl (98+%, Aldrich) solution in de-ionized water
- 0.5 M NaCl (98+%, Aldrich) solution in de-ionized water, de-aerated with nitrogen gas (BayAirgas).
- aerated 0.5 M  $\text{Na}_2\text{SO}_4$  (99%+, J. T. Baker) +0.005 M NaCl (98+%, Aldrich) solution in de-ionized water,

For each test environment, fatigue experiments were repeated two to six times on separate specimens in fresh solution.

All fatigue-crack growth experiments, unless specifically noted, were performed with the sample loaded at a constant load ratio (ratio of minimum to maximum loads) of  $R = 0.1$ , and a frequency of  $\nu = 25$  Hz (sine wave) on an MTS model 831 servo-hydraulic test frame. Testing procedures were in general accordance with ASTM standard E647. Tests were performed under both increasing and decreasing stress-intensity range,  $\Delta K$ , using a stress-intensity gradient of  $\pm 0.1 \text{ mm}^{-1}$  of crack growth; in addition, several tests were performed at a constant cyclic load ( $\Delta P$ ), i.e., under increasing  $\Delta K$  conditions. During cycling, crack lengths were continuously monitored using the unloading elastic compliance, obtained from a back-face strain gauge. Specimens tested in both air and aqueous solution were first pre-cracked in air. For consistency, the pre-cracking procedure was performed in air under identical conditions and was comprised of four loading segments. Each segment consisted of 0.5 mm of crack extension and was carried out under decreasing  $\Delta K$  conditions beginning at  $5.5 \text{ MPa}\sqrt{\text{m}}$ ,  $4.5 \text{ MPa}\sqrt{\text{m}}$ ,  $3.5 \text{ MPa}\sqrt{\text{m}}$ , and finally  $2.5 \text{ MPa}\sqrt{\text{m}}$ , such that the final pre-crack was 2 mm from the notch with a final  $\Delta K$  of  $2.25 \text{ MPa}\sqrt{\text{m}}$ . In cases where fatigue measurements were subsequently performed in an aqueous environment, solution was added while cycling the sample at  $\Delta K$  of  $1 \text{ MPa}\sqrt{\text{m}}$ .

Representative data for each environment are presented as fatigue-crack growth rates per cycle,  $da/dN$ , as a function of the applied stress-intensity range ( $\Delta K = K_{\max} - K_{\min}$ ). The fatigue threshold,  $\Delta K_{\text{TH}}$ , was determined during a decreasing  $\Delta K$  test by allowing the stress-intensity range to decrease until crack-growth rates were near  $10^{-10}$  m/cycle; the value of  $\Delta K_{\text{TH}}$  was then operationally defined as the highest  $\Delta K$  at which  $da/dN < 10^{-10}$  m/cycle.

Most fatigue tests in aqueous solutions were conducted under open-circuit conditions; however, additional testing was performed under potential control in an aerated 0.5 M NaCl solution. During these experiments, the potential was controlled by an EG&G Model 363 potentiostat/galvanostat. Electrical connection was made to the C(T) specimens with an aluminum alloy wire, attached with silver epoxy and subsequently covered with electronically and ionically nonconductive Microstop (Tolber, Hope, AR). After adding about 3 liters of solution to the cell containing the unloaded specimen, the potential of the C(T) specimen was maintained at -2500 mV with a saturated calomel reference electrode (SCE) and a platinum counter electrode for 5 min. After the initial polarization, crack propagation was initiated under open-circuit conditions from the fatigue pre-crack, under sinusoidal loading at  $\Delta K = 1.5 \text{ MPa}\sqrt{\text{m}}$  ( $R = 0.1$ ) with  $\nu = 25$  Hz. After the crack had grown by  $\sim 300 \mu\text{m}$  under open-circuit conditions, potential control at -600 mV was established and crack-growth rates measured. The potential was subsequently stepped down to -800 mV, and back up to +100 mV or +900 mV in 100 mV increments. At each potential, the growth rate was measured during 300  $\mu\text{m}$  to 500  $\mu\text{m}$  of crack growth. On two samples, the potential was held at +900 mV for up to 1 mm of growth, at which point the potential was stepped directly to -900 mV, while time and crack growth were monitored.

Following some of the fatigue-crack growth and stress-corrosion crack growth testing, fracture surfaces were evaluated with scanning electron microscopy and atomic force microscopy (AFM) using an Autoprobe M5 AFM with PSI Proscan Version 1.5 software in tapping mode.

#### IV. Results

The variation in fatigue-crack propagation rates in the bulk amorphous  $Zr_{41.2}Ti_{13.8}Cu_{12.5}Ni_{10}Be_{22}$  alloy as a function of the stress-intensity range is shown in Fig. 1 for environments of laboratory air, aerated de-ionized water and aerated 0.5 M NaCl solution (open circuit). As reported previously [6], growth rates and the fatigue threshold ( $\Delta K_{TH}$ ) are essentially identical in laboratory air and de-ionized water environments. However growth rates in 0.5M aerated NaCl solution are 2 to 3 orders of magnitude faster, rising to a pronounced plateau at  $\sim 5 \times 10^{-7}$  m/cycle at  $\Delta K$  levels between 1 and 6  $MPa\sqrt{m}$  (Fig. 1). Furthermore, compared to behavior in air and de-ionized water, the threshold  $\Delta K_{TH}$  value in NaCl solution is reduced by  $\sim 30\%$  to  $\sim 0.8 MPa\sqrt{m}$ .

Fractographically, the near-threshold fatigue fracture surfaces in 0.5 M NaCl appeared smooth and optically reflective over large areas (larger than 1  $mm^2$  in some instances), as shown in the SEM image in Fig. 2a. Further AFM imaging in Fig. 2b, showed that these smooth areas have roughnesses below 100 nm, and are separated by steps, 0.1 to 50  $\mu m$  in height. With crack extension and decreasing stress-intensity range, these steps either merge together to form larger ones or decrease in height until they disappear.

Further insight into this dramatic environmentally-assisted cracking phenomenon in this alloy was sought by systematically varying the loading cycle, stress-intensity range, solution concentration, anion identity, solution de-aeration, and bulk electrochemical potential; results are described below.

*Stress-intensity range:* For all aqueous NaCl solutions, the stress-intensity range was varied and crack-growth rates measured. In all cases, there was a distinct  $\Delta K_{TH}$  threshold below 1  $MPa\sqrt{m}$ , a Region I regime where growth rates increased dramatically by 2 to 4 orders of magnitude, followed by a Region II (plateau) regime where growth rates were essentially constant and did not depend significantly on the  $\Delta K$  level (Fig. 3).

*Loading cycle:* Fatigue-crack growth rates in aerated 0.5 M NaCl solution were measured at four sinusoidal frequencies (2.5, 10, 25 and 50 Hz) and four load ratios ( $R = 0.1, 0.3, 0.5$  and 0.7) at a constant  $\Delta K$  of 1.2  $MPa\sqrt{m}$  (in Region II) to compare to the stress-corrosion cracking behavior; results are shown in Figs. 4a and 4b, respectively. It is apparent that

crack-growth rates per cycle are significantly reduced with increasing frequency, yet are only slightly increased with increasing load ratio.

*Sodium chloride concentration:* Fatigue-crack growth rates in the Region II (plateau) regime in aerated aqueous solutions were found to be a function of the concentration of sodium chloride (Fig. 3). Specifically, steady-state growth rates were decreased from  $\sim 5 \times 10^{-7}$  to  $\sim 1.5 \times 10^{-8}$  m/cycle with a decrease in the sodium chloride concentration from 0.5 M to 0.005 M NaCl, establishing a dependence of fatigue-crack growth rates on chloride concentration. However, the value of fatigue threshold varied insignificantly over three orders of magnitude in sodium chloride concentration. Specifically,  $\Delta K_{TH}$  was constant at  $\sim 0.84$  MPa $\sqrt{m}$  when the sodium chloride concentration is 0.5 M, 0.05 M, or 0.005 M (Fig. 3).

*Anion identity:* Fatigue-crack growth rates in Region II were approximately an order of magnitude lower in the presence of ClO<sub>4</sub><sup>-</sup> anions (in 0.5 M sodium perchlorate solution) and SO<sub>4</sub><sup>2-</sup> anions (in 0.5 M sodium sulfate solution), compared to corresponding growth rates in the presence of Cl<sup>-</sup> anions (in 0.5 M NaCl) (Fig. 5). In addition,  $\Delta K_{TH}$  thresholds were found to be 1.0 and 1.2 MPa $\sqrt{m}$ , respectively, in sodium sulfate and sodium perchlorate solutions, i.e., 25 to 50% higher than the fatigue threshold of 0.8 MPa $\sqrt{m}$  measured in sodium chloride solutions.

*Solution aeration and de-aeration:* A 0.5 M NaCl solution open to air was compared to behavior in a 0.5 M NaCl solution, de-aerated by bubbling with nitrogen gas. The presence of oxygen (i.e., exposed to air at 1 atm) in the aqueous solution had an insignificant effect on Region II fatigue-crack growth rates and the value of the fatigue threshold (Fig. 6).

*Potential control:* To attempt to isolate the salient mechanisms of stress-corrosion fatigue-crack propagation in sodium chloride solution, the amorphous metal was polarized to potentials between -900 mV (SCE) and +900 mV (SCE) during cyclic fatigue tests in 0.5 M NaCl. In Fig. 7, resulting crack-growth rates at a constant  $\Delta K$  in air of 1.5 MPa $\sqrt{m}$  (region II) are plotted as a function of potential, where it can be seen that growth rates decrease rapidly from a high of  $\sim 10^{-6}$  to  $10^{-7}$  m/cycle as the specimen is polarized cathodically below -750 mV (SCE). Although the potential was stepped during the continuous growth of a fatigue crack, fatigue-crack growth rates stabilized after less than

100  $\mu\text{m}$  of crack extension after each 100 mV step. Furthermore, no crack growth was observed in 24 hrs at -900 mV.

The potential also markedly affects the fatigue threshold. In Fig. 8, the threshold stress intensity,  $\Delta K_{\text{TH}}$ , for amorphous  $\text{Zr}_{41.2}\text{Ti}_{13.8}\text{Cu}_{12.5}\text{Ni}_{10}\text{Be}_{22.5}$  in 0.5 M NaCl is shown to decrease in two steps, as the bulk polarization potential becomes more anodic<sup>2</sup>. Specifically, between -1000 mV and -850 mV,  $\Delta K_{\text{TH}}$  in 0.5M NaCl is about 1.5  $\text{MPa}\sqrt{\text{m}}$ , which is approximately the threshold value in air and de-ionized water. At -800 mV, however,  $\Delta K_{\text{TH}}$  drops sharply to about 0.9  $\text{MPa}\sqrt{\text{m}}$ , which is approximately the threshold at open circuit in 0.5 M NaCl. Between -800 mV and -200 mV,  $\Delta K_{\text{TH}}$  appears to decrease slightly to about 0.76  $\text{MPa}\sqrt{\text{m}}$ . Finally, between -200 mV and 0 mV, the  $\Delta K_{\text{TH}}$  threshold drops sharply again to an extremely low value of  $\sim 0.3 \text{MPa}\sqrt{\text{m}}$ . It should be noted that even under open circuit conditions, these threshold values in aqueous NaCl solution are extremely low (by more than one order of magnitude) compared to the fracture toughness of the alloy, which (depending upon strain rate) varies between 12 and 70  $\text{MPa}\sqrt{\text{m}}$  [1].

## V. Discussion

Studies on stress corrosion and corrosion fatigue behavior of amorphous  $\text{Zr}_{41.2}\text{Ti}_{13.8}\text{Cu}_{12.5}\text{Ni}_{10}\text{Be}_{22.5}$  have demonstrated a *major* effect of aqueous sodium chloride solutions in accelerating fatigue-crack propagation rates and reducing fatigue threshold values in the fully amorphous alloy [6]. In this paper, a more detailed investigation of this effect has shown that such environmentally-assisted fatigue-crack growth rates depend strongly on the cyclic frequency (Fig. 4a), the chloride concentration (Fig. 3), the anion character (Fig. 5), and the extent of cathodic polarization (Fig. 7), and also depend weakly on the (positive) load ratio (Fig. 4b). However, these growth rates do not depend on the stress-intensity range (Fig. 3), or on the solution aeration (Fig. 6), in the steady-state (plateau) regime above the threshold. Near the fatigue threshold, growth rates drop

---

<sup>2</sup> Although the bulk polarization potential is controlled and recorded in Fig. 7 and Fig. 8, the crack-tip potential lies between the corrosion potential and the applied bulk potential, and scales in value with the bulk potential [16]. In this study, the C(T) specimens were externally polarized, rather than directly polarized at the crack tip. Since the crack tip is occluded and it is likely that concentration gradients exist, importance will not be attached to the absolute value of potential, but the direction of polarization, either anodic or cathodic from the corrosion potential is considered significant.

precipitously with stress-intensity range, but do not depend on chloride concentration (Fig. 3). These dependencies are summarized in Table 2.

To explain this behavior, a mechanism of stress-assisted, anodic dissolution for environmentally-assisted fatigue-crack propagation in the amorphous Zr-Ti-Cu-Ni-Be alloy is proposed. Further, rate-determining steps for such behavior are reasoned to be electrochemical, stress-dependent reaction at near-threshold levels, and mass transport at higher (steady-state) growth rates.

**Table 2:** The dependence of fatigue-crack growth rates on stress-intensity range, chloride concentration, anodic potential, anion character, and cathodic potential in the near-threshold and higher growth-rate regimes.

$\Delta K$ regime	Stress-intensity range	Chloride concentration	Anodic Potential	Anion Identity	Cathodic Potential
Near-threshold (Region I)	Dependent	Independent	Dependent	Dependent	Dependent
Above threshold (Region II)	Independent	Dependent	Independent	Dependent	Dependent

### V.1. Stress-corrosion cracking and fatigue

The environmentally-assisted contribution to fatigue-crack growth rates in the amorphous Zr-Ti-Cu-Ni-Be alloy in aqueous NaCl solution can be attributed to a stress-corrosion cracking process, which is observed under constant (non-cyclic) loads in the same solution [17]. Indeed, experimentally measured crack velocities, acquired during constant-load, stress-corrosion cracking (SCC) tests in 0.5 M NaCl (open circuit), can be used directly to predict the fatigue-crack growth rates in this solution using *superposition* [18] or *process-competition* [19-20] models. Specifically, fatigue-crack growth rates in 0.5 M NaCl,  $(da/dN)_{\text{eff}}$ , are calculated by integrating the stress-corrosion crack velocities,  $(da/dt(K(t)))_{\text{SCC}}$ , over the time,  $t$ , of one fatigue cycle [18, 21] where  $\nu$  is the cyclic loading frequency [17]:

$$\left(\frac{da}{dN}\right)_{\text{eff}} = \int_0^{1/\nu} \left(\frac{da}{dt}(K(t))\right)_{\text{SCC}} dt. \quad (1)$$

These predictions are consistent with the experimentally measured fatigue-crack propagation rates, implying that crack growth in amorphous  $Zr_{41.2}Ti_{13.8}Cu_{12.5}Ni_{10}Be_{22.5}$  under cyclic fatigue loading in NaCl solution results principally from a (non-cyclic) SCC mechanism. Indeed, the same smooth, optically reflective fracture surfaces (Fig. 2) are seen during both stress-corrosion cracking and fatigue-crack growth.

Using Eq. 1, fatigue-crack growth rates in 0.5 M NaCl at a constant  $\Delta K$  of 1.2 MPa $\sqrt{m}$  may be predicted as a function of frequency and load ratio, as shown in Figs. 4a-b, respectively. In fact, the predicted trends from the superposition and process-competition models (Eq. 1) show a decrease in growth rates with increasing frequency and decreasing load ratio, in reasonable consistency with experimental results. However, the model predictions are less accurate at low frequencies and high load ratios where predicted growth rates are higher than those measured experimentally.

The mechanistic relationship between SCC and corrosion fatigue is also consistent with the experimental result that the aerated and de-aerated 0.5M NaCl solutions yield the same stress-corrosion fatigue behavior (Fig. 6). In an aerated solution, an oxygen gradient may exist between the bulk solution and the crack tip that could result in a potential difference that could drive SCC. However, this oxygen gradient would likely be disturbed with cycling, such that SCC behavior would overestimate stress-corrosion fatigue behavior if solution aeration were significant to the SCC mechanism.

## V.2. Anodic mechanism

At open circuit, immersion in sodium chloride solution leads to very high Region II fatigue-crack growth rates (Fig. 1). However, cathodic polarization reduces or eliminates crack growth (Fig. 7). This potential dependence strongly suggests an anodic mechanism of crack growth, which is effectively stopped at potentials more cathodic than -900 mV (SCE).

For the Zr-Ti-Cu-Ni-Be alloy, the fastest crack-growth rates are observed in the presence of the most aggressive anions, the chloride ions. Growth rates were an order of magnitude or more faster in 0.5 M NaCl than in 0.5 M Na<sub>2</sub>SO<sub>4</sub> or 0.5 M NaClO<sub>4</sub> solutions (Fig. 5). The Cl<sup>-</sup> ion is the most aggressive, consistent with its high mobility, high charge

density, small radius, and lack of hydration [22].<sup>3</sup> The higher crack-growth rate in the chloride solution can be related to either the higher mobility of Cl<sup>-</sup> in a mass transport-limited system (see the RDS section), the rate of reaction at the crack tip, or the strength of adsorption at the crack tip. This anion dependence is also consistent with an anodic mechanism.

There are several anodic processes that could be responsible for SCC, including film rupture/slip step dissolution, de-alloyed layer crack initiation, and active dissolution (reviewed in ref. [23]). With reference to the amorphous Zr-Ti-Cu-Ni-Be alloy, active dissolution is clearly the most likely mechanism because the stress-corrosion fatigue-crack growth rates can be directly predicted from the SCC rates. The film rupture/slip step dissolution mechanism is less feasible as it would be strongly affected by cycling, which creates more plastic deformation than static SCC. Similarly, the de-alloyed layer/crack initiation mechanism is also unlikely to be active here as the proportion of elements that would go into the aqueous solution at open circuit (Cu and Ni) is too low to form a voided layer to percolate the solution; moreover, no evidence of such a layer, which should be a micrometer or so wide, was detected by SEM examination of the surface [24].<sup>4</sup> For active dissolution, an oxide does not protect the metal at the crack tip, often because an aggressive local environment is established there. To prevent blunting of the crack tip by this dissolution, crack growth must be fairly fast, as it is for the amorphous Zr-Ti-Cu-Ni-Be alloy.

A cathodic (hydrogen-based) mechanism of crack growth is also not supported by the experimental results, specifically that cathodic polarization effectively prevented corrosion fatigue in this alloy. Indeed, cathodic polarization was used to stop crack growth for 24 hr, which upon subsequent anodic polarization grew immediately. In an earlier study,

---

<sup>3</sup> Charge density and size of the anion is particularly relevant to the value of the threshold  $\Delta K_{TH}$ . These attributes may affect the proximity of the inner Helmholtz plane (IHP) of unhydrated ions adjacent to the metal surface. A change in the distance to the IHP can result in a change in the potential gradient (experienced by oxidizing metal atoms) at the interface between the metal and solution.

<sup>4</sup> The rate of SCC is roughly two orders of magnitude faster than the rate of de-alloying [25]. For this mechanism to activate, ~20 - 60 at.% of the metallic atoms must preferentially oxidize, so that the porous layer may percolate with solution [23,25]. In the Zr-Ti-Cu-Ni-Be alloy, Zr, Ti and Be may preferentially oxidize, but consist of 77% of the metal.

hydrogen charging of Zr-Ti-Cu-Ni-Be was found to increase the slope of the  $da/dN$  vs.  $\Delta K$  curve and increase the fatigue threshold [26]. Such a slope change was not observed in the current experiments. Furthermore, in aqueous solution, the fatigue threshold was decreased relative to the threshold in air.

*Consistency of near-threshold behavior with mechanism:* The fatigue threshold depends on the polarization of the specimen, which is consistent with an anodic dissolution mechanism. In fact, the potential dependence suggests activation of particular dissolution reactions. In Fig. 8, the  $\Delta K_{TH}$  threshold stress intensity is shown to decrease in two steps, as the polarization potential becomes more anodic. These steps occur at cathodic potentials of  $-850$  mV (SCE) and  $-200$  mV (SCE).

For a specific oxidation reaction, an increase in anodic polarization decreases the energy for an anodic charge transfer oxidation reaction by increasing the energy of atoms in the metal, i.e., increasing the thermodynamic driving force for ionizing a metal atom. In this case, however, the dependence on potential occurs in two steps (see Fig. 8). The step-like nature of the dependence of threshold on potential does not suggest a Tafel or even linear dependence of a single reaction on potential; it suggests that either a particular anodic reaction is activated or a critical reaction rate is attained above the step potential of  $-850$  mV and  $-200$  mV.

The steps at  $-850$  mV and  $-200$  mV may correspond to activation of Ni and Cu electrochemical dissolution reactions. In pure form, the Pourbaix diagram predicts that pure Ni is stable below  $\sim -640$  mV (SCE) and pure Cu is stable below  $\sim -100$  mV for the bulk solution pH [27]. The difference between the predicted and measured potentials for these reactions may be related to the fact that these metals are alloyed, or the fact that a potential drop occurs between the bulk solution and the crack tip. Hence, polarization affects the active dissolution reactions, which in turn affect the stress-intensity range at which stress-corrosion fatigue occurs.

### **V.3. Rate-determining steps (RDS)**

The dependence of fatigue-crack growth rates on various mechanical, chemical, and electrochemical factors is summarized in Table 2. This set of dependencies may be used to assess the rate-determining steps (RDS) for crack growth.

*RDS above the threshold:* At stress-intensity ranges above the fatigue threshold (region II), crack-growth rates are largely independent of both the mechanical driving force (Fig. 3) and electrochemical driving force at anodic potentials (Fig. 7), yet dependent on chloride concentration. A rate-determining step of mass transport is consistent with these dependencies. A dependence on chloride concentration suggests a mass transport limitation or a reaction-rate dependence on chloride ions, i.e., to a stress-assisted, anodic dissolution mechanism. Since the growth rates do not depend on potential, mass transport is the likely RDS. A higher bulk concentration can lead to a greater concentration gradient and an increase in ionic flux to and from the crack tip.

The independence of growth rates on potential over a range of anodic potentials (Fig. 7) suggests that the electrochemical reaction itself is not the rate-determining step. If an anodic reaction is rate-limiting, then crack-growth rates would be expected to increase as anodic polarization increases, based on the Butler-Volmer relation [28-29] between current density and over potential. If the RDS were an electrochemical reaction, then the crack-growth rates, by relation to the current density, would have a linear or exponential relationship with potential. This Tafel or linear dependence is not reflected in the growth-rate data above the corrosion potential between 0 and 1000 mV (Fig. 7). This lack of dependence on anodic polarization may be attributed to a rate-determining step that does not involve charge transfer.

*RDS at near-threshold levels:* Although the crack-growth mechanism at near-threshold stress intensities is likely to be the same as at higher growth rates in region II, the rate-determining step may differ. This change in rate-determining step is reflected in the markedly different dependency of crack-growth rates on stress-intensity range, electrochemical potential, and chloride concentration in these two regimes (see Table 2). Specifically near the threshold, crack-growth rates depend on anodic potential, stress-intensity range, and anion identity, but not on chloride concentration.

Strain, potential, and anion type change the energy barrier for electrochemical reactions at the crack tip. These three parameters can change whether a reaction is favorable or not. Chloride concentration may have a similar impact through the Nernst equation that relates potential to concentration [30]. However, the potential change will be small between 0.005 M and 0.5M of chloride ions. For a first-order reaction, the potential

difference would be about 110 mV, which may not be significant in light of the step dependence of the threshold on potential shown in Fig. 8. The threshold is relatively stable over a 600 mV range. The magnitude of the impact on the energy barrier may be larger in response to changes in stress intensity, potential, and anion identity, than to changes in chloride concentration.

Mass transport has been proposed above as a possible rate-determining step for stress-corrosion fatigue-crack growth rates at stress intensities above the threshold regime. However, this rate-determining step would not be likely near the fatigue threshold because slow crack growth rates allow time for diffusion to and from the crack tip. It appears that a stress-assisted electrochemical reaction is rate-determining near the fatigue and stress-corrosion cracking thresholds because a change in either potential or stress intensity can rapidly decrease the rate of crack growth.

#### **V.4. Rapid corrosion crack growth in an amorphous metal**

It is often assumed that amorphous metals have far better corrosion resistance than crystalline materials because of their structural and chemical homogeneity. However, amorphous metals do not always exhibit superior corrosion resistance in experiments. In fact, prior potentiodynamic polarization studies (in 0.5 M NaCl and 0.5 M NaClO<sub>4</sub> solutions) on the current alloy in the crystalline and amorphous states indicated that the amorphous structure was only marginally more resistant to pitting corrosion in an NaCl solution and no more resistant to general corrosion in an NaClO<sub>4</sub> solution [31]. Experiments suggest that the presence of the amorphous phase does not necessarily guarantee superior corrosion resistance. In addition to the amorphous structure, excellent corrosion resistance has been attributed to the presence of a highly stable, rapidly repairing, passive film, concentrated in certain alloying elements known to provide good corrosion resistance in crystalline metals [32-33].

In earlier studies, amorphous metals have exhibited stress-corrosion cracking [11]; however, the acceleration in growth rates due to the presence of an active environment was nowhere near as significant as seen in the current Zr-based alloy. It is thus interesting to consider why environmentally-assisted crack-growth rates are so fast in this amorphous alloy [6]. Two factors may explain this. First, the fracture-mechanics tests used in the

current study to evaluate SCC are far more discerning than the loading of smooth amorphous ribbons used in earlier studies [11-15,34]. In this earlier work, crack initiation and crack growth were coupled in the same test, such that the results yield little information on the respective crack-growth rates. Second, the oxide layer for the Zr-Ti-Cu-Ni-Be metal is quite distinct from that of the amorphous metals where previous corrosion studies have been reported. Specifically, much of the earlier work was performed on Fe-based amorphous alloys. Good SCC resistance was observed in alloys that showed good resistance to pitting corrosion in the absence of load [11-14]. This resistance to pitting corrosion suggests a passivating film that can heal rapidly. In some cases, the Fe-based amorphous alloys were alloyed with Cr, known for its corrosion resistance [11]. Moreover, in another study SCC resistance of amorphous  $\text{Fe}_{40}\text{Ni}_{38}\text{Mo}_4\text{B}_{18}$  in HCl was attributed to its good passivity, while a group of Fe-based, Fe-B-Si, amorphous metals exhibited SCC in 25-100% HCl solutions [34]. In the Zr-Ti-Cu-Ni-Be alloy, conversely, the air-formed oxide layer appears to be a mix of metallic oxides, predominantly  $\text{ZrO}_2$  [24]; as these oxides would not provide as much corrosion protection as a Cr-based film, the resulting contribution to crack growth from SCC is likely to be much more significant.

We conclude from this that from the general perspective of developing superior resistance to localized corrosion and stress-corrosion cracking, it is the composition of the alloy that is more important than whether the structure is crystalline or amorphous.

## VI. Summary and Conclusions

Based on an experimental study of stress-corrosion fatigue-crack growth in aqueous salt solutions in a fully amorphous  $\text{Zr}_{41.2}\text{Ti}_{13.8}\text{Cu}_{12.5}\text{Ni}_{10}\text{Be}_{22.5}$  alloy, the results can be summarized as follows:

1. Fatigue-crack growth rates were found to be as much as three orders of magnitude higher in aqueous 0.5 M NaCl solution under open-circuit conditions, compared to corresponding behavior in laboratory air or de-ionized water. Corresponding fatigue
2. Fatigue-crack growth behavior ( $da/dN$  vs.  $\Delta K$ ) in the aqueous solutions was seen to display an abrupt threshold, whereupon the growth rates increased by 3 to 5 orders of

magnitude to reach a plateau (Region II) regime where crack growth is essentially independent of the stress-intensity range. Compared to a value of the fatigue threshold in air of almost  $3 \text{ MPa}\sqrt{\text{m}}$ , the value of  $\Delta K_{\text{TH}}$  in the aqueous solution was markedly reduced to  $\sim 0.9 \text{ MPa}\sqrt{\text{m}}$ . This fatigue threshold in aqueous solution is more than an order of magnitude lower than the fracture toughness of the alloy.

3. Similar behavior was seen under constant (non-cyclic) loading conditions, where crack growth by stress-corrosion was seen to occur above a  $K_{\text{TH}}$  threshold of  $\sim 0.9 \text{ MPa}\sqrt{\text{m}}$  and to markedly increase 3 to 5 orders of magnitude to reach a (constant velocity) plateau region at growth rates of  $\sim 4 \times 10^{-5} \text{ m/s}$ .
4. The constant fatigue-crack growth rates in Region II were directly proportional to the concentration of NaCl in solution, based on open-circuit testing in 0.5 M, 0.05 M and 0.005 M solutions; the  $\Delta K_{\text{TH}}$  threshold values, however, remained relatively unaffected. Growth rates were about an order of magnitude slower in 0.5 M NaClO<sub>4</sub> and 0.5 M Na<sub>2</sub>SO<sub>4</sub> solutions under open-circuit conditions, compared to behavior in 0.5 M NaCl. Fatigue-crack growth rates in 0.5 M NaCl were unaffected by solution aeration, compared to de-aeration with nitrogen gas.
5. Under potential control conditions, growth rates in this solution decreased to zero at cathodic potentials of about -900 mV, but did not change significantly between -200 mV and +900 mV (SCE).

Based on these observations, it is concluded that the marked environmentally-assisted contribution to fatigue-crack growth in aqueous sodium chloride solution can be attributed to a stress-corrosion crack-growth mechanism. This mechanism appears to involve stress-assisted, anodic dissolution at the crack tip. The rate-determining steps for this mechanism appear to be associated with a charge transfer reaction at near-threshold stress intensities, and the mass transport of metallic ions from the corroding crack tip at higher stress intensities. The poor environmentally-cracking resistance of this amorphous metal may be related primarily to its composition, as this does not yield a strongly protective oxide at the crack tip, and to the relatively thermodynamically unstable nature of its amorphous structure.

## Acknowledgments

This work was supported by the Director, Office of Science, Office of Basic Energy Sciences, Division of Materials Sciences and Engineering of the U.S. Department of Energy under Contract No. DE-AC02-05CH11231. Thanks are due to Amorphous Technologies International, Corp. (Laguna Niguel, CA) for supplying the material.

## References

1. Gilbert CJ, Schroeder V, Ritchie RO. *Metall Mater Trans A* 1999; 30A: 1739.
2. Gilbert CJ, Ritchie RO, Johnson WL. *Appl Phys Lett* 1997; 71: 476.
3. Wang GY, Liaw PK, Peter WH, Yang B, Yokoyama Y, Benson ML, Green BA, Kirkham MJ, White SA, Saleh TA, McDaniels RL, Steward RV, Buchanan RA, Liu CT, Brooks CR. *Intermetallics* 2004; 12: 885.
4. Wang GY, Liaw PK, Peter WH, Yang B, Freels M, Yokoyama Y, Benson ML, Green BA, Saleh TA, McDaniels RL, Steward RV, Buchanan RA, Liu CT, Brooks CR. *Intermetallics* 2004; 12: 1219.
5. Hess PA, Dauskardt RH. *Acta Mater* 2004; 52: 3525.
6. Schroeder V, Gilbert CJ, Ritchie RO. *Scripta Mater* 1999; 49: 1057.
7. Naka M, Hashimoto K, Masumoto T. *Corrosion* 1976; 32: 146.
8. Devine TM. *J Electrochem Soc* 1977; 124: 1.
9. Mansour AN, Melendres CA. *J Electrochem Soc* 1995; 142: 1961.
10. Ramchandran T, Namboodhiri TKG. *Corrosion* 1984; 40: 73.
11. Jones RH, Wang R. *Corrosion* 1986; 42: 504.
12. Archer MD, McKim RJ. *Corrosion* 1983; 39: 91.
13. Kawashima A, Hashimoto K, Masumoto T. *Corrosion Sci* 1976; 16: 935.
14. Sandenbergh RF, Latanision RM. *Corrosion* 1985; 41: 369.
15. Habib K. *Scripta Metall Mater* 1994; 31: 1669.
16. Turnbull A, Dolphin AS, Rackley FA. *Corrosion* 1988; 44: 55.
17. Schroeder V, Gilbert CJ, Ritchie RO. *Mater Sci Eng A* 2001; 317: 145.
18. Wei RP, Landes JD. *Mater Res Stand* 1969; 9: 25.
19. Austen IM, Walker EF. In: *International Conference on the Influence of the Environment*, ImechE; 1977: p. 1.
20. Austen IM, McIntyre P. *Metal Sci* 1979: 420.
21. Bucci RJ. Masters Thesis, Lehigh University, 1970.

22. Jones DA, Principles and Prevention of Corrosion, Macmillan Publishing Co., New York, New York, 1992.
23. Newman RC. In: Marcus P, Oudars J, editors. Corrosion Mechanisms in Theory and Practice, Marcel Dekker Inc., New York, New York, 1995, p.311
24. Schroeder V, Doctoral Dissertation, U.C. Berkeley, 2000.
25. Sieradzki K, Kim JS, Cole AT, Newman RC. J Electrochem Soc 1987; 134: 1635.
26. Suh D, Dauskardt RH. Scripta Mater 2000; 42: 233
27. Pourbaix M, Atlas of Electrochemical Equilibria in Aqueous Solutions, Pergamon Press, Oxford, U. K., 1966.
28. Erdey-Gruz T, Volmer M. Z Physik Chem 1930; 150A: 203.
29. Butler JAV. Proc Roy Soc 1936; A157: 423.
30. Nernst W. Z Physik Chem 1904; 47: 52.
31. Schroeder V, Gilbert CJ, Ritchie RO. Scripta Mater 1998; 38: 1481.
32. Hashimoto K. In: Froment M, editor. Passivity of Metals and Semiconductors, Elsevier Sci. Publ., Amsterdam, 1984, p. 235.
33. Virtanen S, Bohni H. Corrosion Sci 1990; 31: 333.
34. Habib K, Nessler R, Moore K. Corrosion 1993; 49: 619.

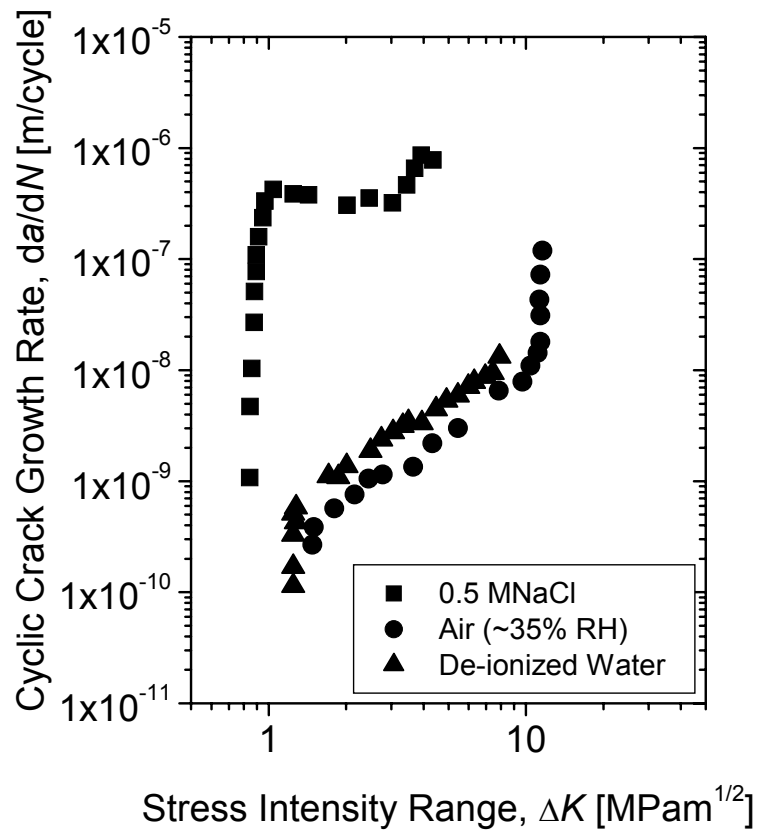


Figure 1. Fatigue-crack growth rates (under sinusoidal loading) in amorphous  $Zr_{41.2}Ti_{13.8}Cu_{12.5}Ni_{10}Be_{22.5}$  are plotted as a function of the stress-intensity range,  $\Delta K$ , for three environments: aerated 0.5 M NaCl solution, de-ionized water, and laboratory air (relative humidity of 30-35%).

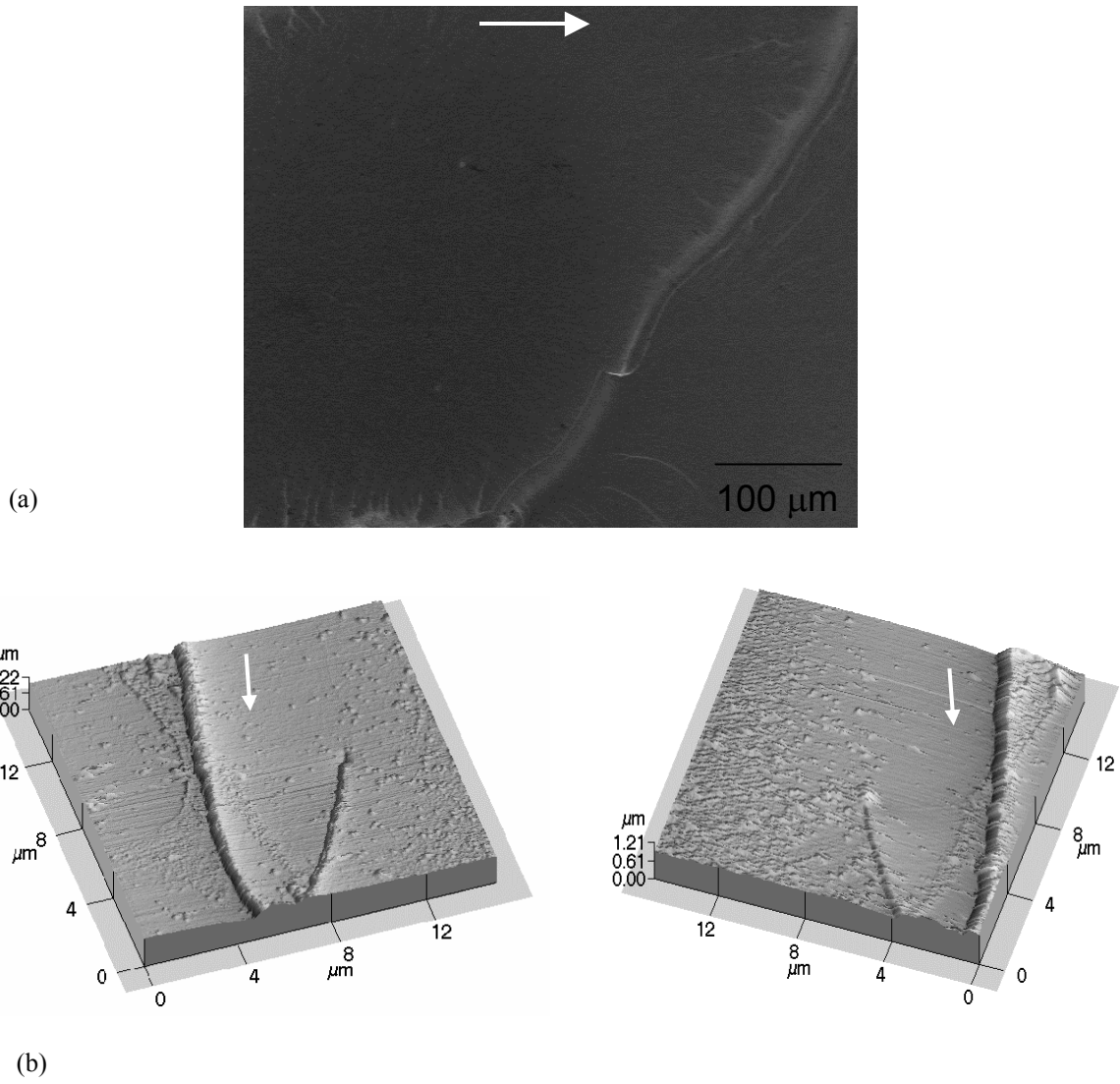


Figure 2. (a) Scanning electron microscope image of amorphous  $Zr_{41.2}Ti_{13.8}Cu_{12.5}Ni_{10}Be_{22.5}$  fracture surface created by corrosion fatigue-crack growth in an aqueous 0.5 M NaCl solution at near-threshold levels, and (b) matching atomic force microscopy images. The white arrows indicate the crack-growth directions.

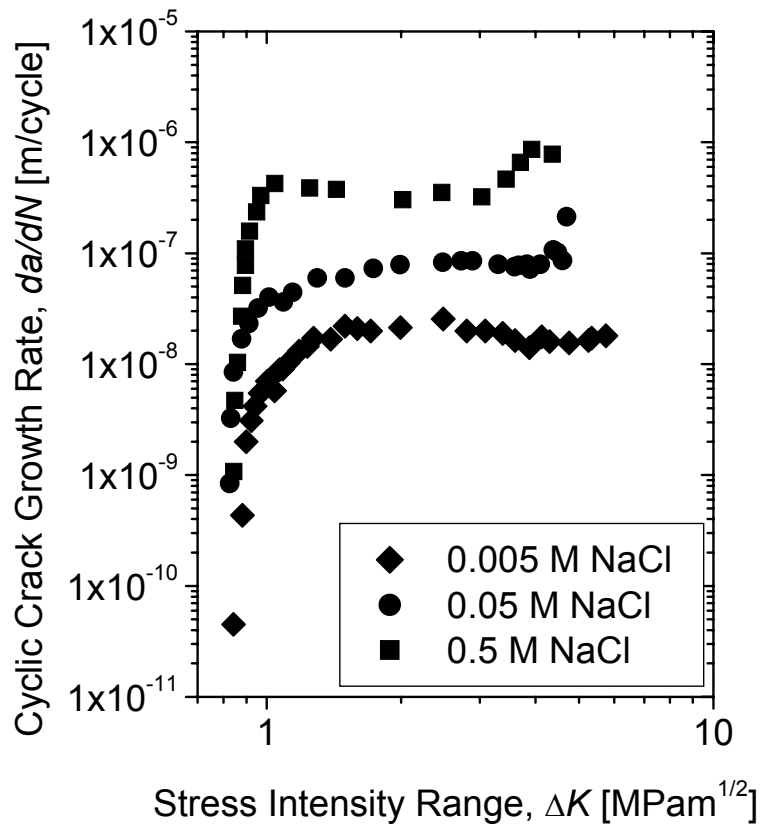


Figure 3. Fatigue-crack growth rates (under sinusoidal loading) in amorphous  $\text{Zr}_{41.2}\text{Ti}_{13.8}\text{Cu}_{12.5}\text{Ni}_{10}\text{Be}_{22.5}$  are plotted as a function of the stress-intensity range,  $\Delta K$ , for three environments: aerated 0.5 M, 0.05M, and 0.005 M NaCl solutions.

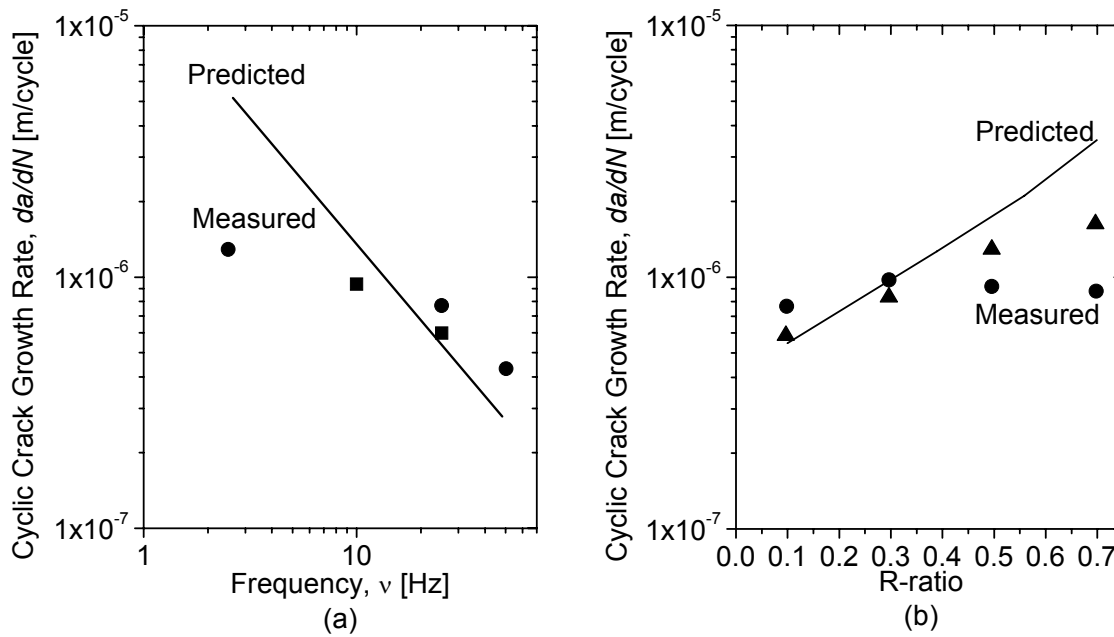


Figure 4. Fatigue-crack growth rates (under sinusoidal loading) in amorphous  $Zr_{41.2}Ti_{13.8}Cu_{12.5}Ni_{10}Be_{22.5}$  in an aerated 0.5 M NaCl solution at constant  $\Delta K = 1.2 \text{ MPa}\sqrt{\text{m}}$ , at variable (a) frequency and (b)  $R$ -ratio, recorded during 0.5-1 mm of crack growth at each condition during two separate tests.

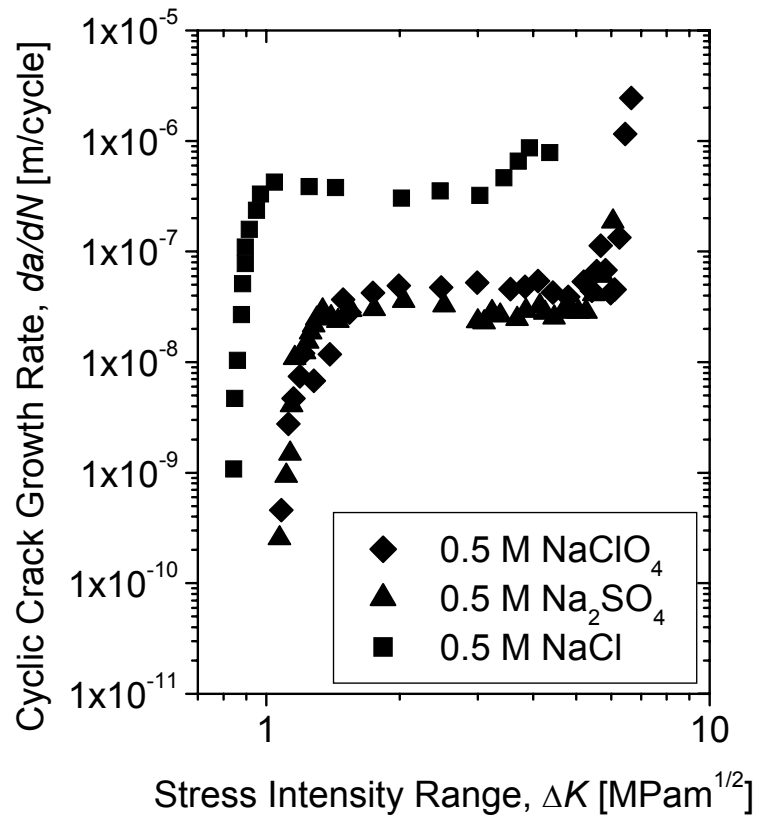


Figure 5. Fatigue-crack growth rates (under sinusoidal loading) in amorphous  $Zr_{41.2}Ti_{13.8}Cu_{12.5}Ni_{10}Be_{22.5}$  are plotted as a function of the stress-intensity range,  $\Delta K$ , for three environments: aerated 0.5 M NaCl, 0.5 M NaClO<sub>4</sub>, and 0.5 M Na<sub>2</sub>SO<sub>4</sub> solutions.

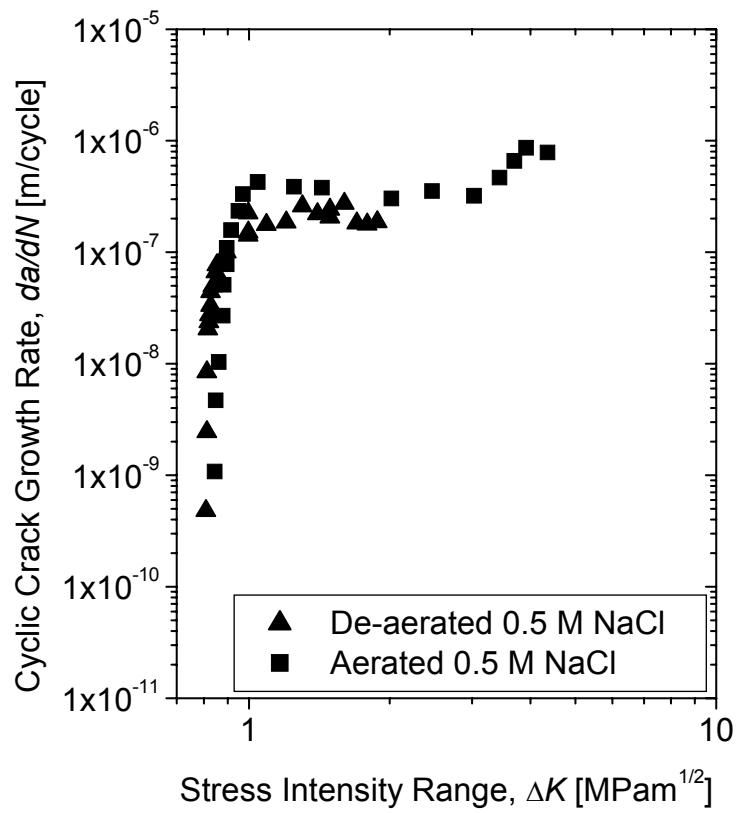


Figure 6. Fatigue-crack growth rates (under sinusoidal loading) in amorphous  $\text{Zr}_{41.2}\text{Ti}_{13.8}\text{Cu}_{12.5}\text{Ni}_{10}\text{Be}_{22.5}$  are plotted as a function of the stress-intensity range,  $\Delta K$ , for two environments: aerated and de-aerated 0.5 M NaCl solutions.

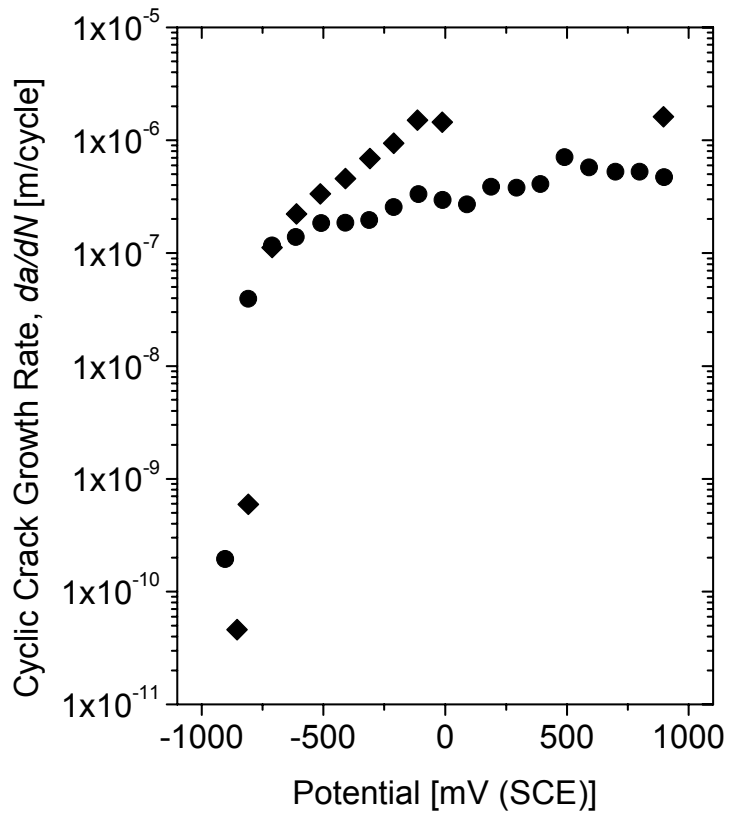


Figure 7. Fatigue-crack growth rates (under sinusoidal loading) in amorphous  $Zr_{41.2}Ti_{13.8}Cu_{12.5}Ni_{10}Be_{22.5}$  in an aerated 0.5 M NaCl solution under potential control at constant  $\Delta K = 1.2 \text{ MPa}\sqrt{\text{m}}$ , recorded during 0.3-0.5 mm of crack growth at each potential during two separate tests.

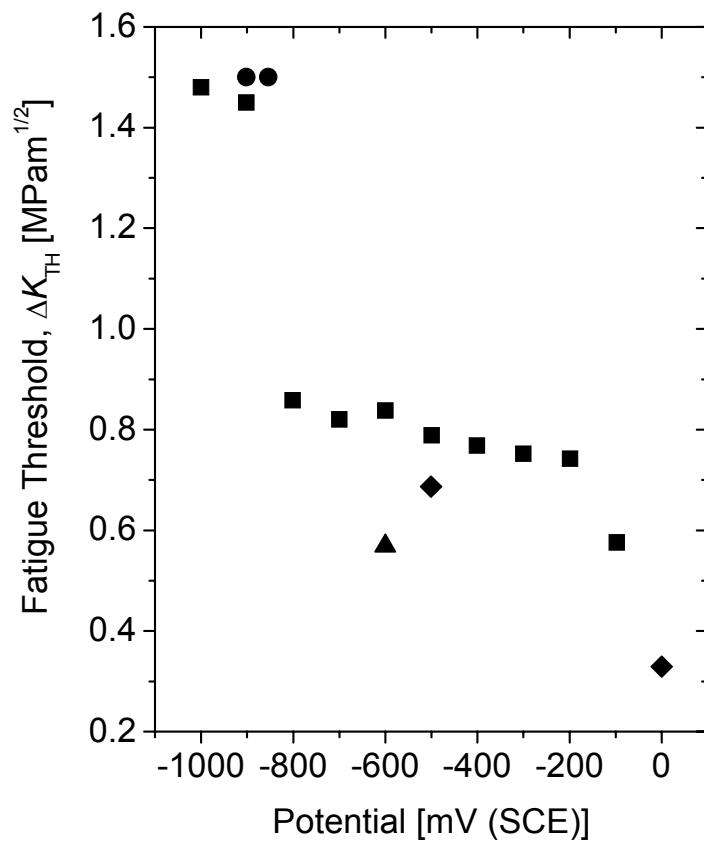


Figure 8. Fatigue thresholds measured at fatigue-crack growth rates below  $3 \times 10^{-9}$  m/cycle in amorphous  $Zr_{41.2}Ti_{13.8}Cu_{12.5}Ni_{10}Be_{22.5}$  in an aerated 0.5 M NaCl solution under potential control in five separate tests.